Pergamon

Int. J. Multiphase Flow Vol. 24, No. 4, pp. 523–537, 1998

Printed in Great Britain
PII: S0301-9322(97)00084-0
0301-9322/98 $19.00 + 0.00

MEAN VELOCITY AND TURBULENCE CHARACTERISTICS OF WATER FLOW IN THE BUBBLE DISPERSION REGION INDUCED BY PLUNGING WATER JET

M. IGUCHI[1], K. OKITA[2] , and F. Yamamoto[3]

[1]Division of Materials Science and Engineering, Graduate School of Engineering, Hokkaido University, North 13, West 8, Kita-ku, Sapporo, Hokkaido, 060 Japan
[2]Graduate School of Engineering, Hokkaido University, North 13, West 8, Kita-ku, Sapporo, Hokkaido, 060 Japan
[3]Department of Mechanical Engineering, Faculty of Engineering, Fukui University, 3-9-1 Bunkyo, Fukui, Fukui, 910 Japan

(Received 3 May 1997; in revised form 23 October 1997)

Abstract—Water was injected vertically downward through a straight circular pipe onto a water bath contained in a cylindrical vessel. Three types of bubble dispersion patterns were observed with respect to the distance from the pipe exit to the undisturbed bath surface. When the distance was short, small bubbles were generated at the bath surface and they dispersed in the whole bath (type 1). On the other hand, when the distance was long, relatively large bubbles were generated and the bubble dispersion region was localized beneath the pipe exit (type 3). For an intermediate distance, the bubble dispersion patterns of the two types appeared simultaneously (type 2). We focused on types 1 and 3 and carried out LDV measurements to investigate the liquid motion in the bubble dispersion region. In the case of type 1, the mean velocity and turbulence characteristics were not affected by bubbles and agreed well with those for single-phase free jets, while the two characteristics for type 3 were influenced significantly by bubbles. The differences in the two characteristics between types 1 and 3 were found to be associated with turbulence production in the wake of bubbles. © 1998 Elsevier Science Ltd. All rights reserved

Key Words: two-phase flow, LDV, plunging jet, bubbling jet, turbulence, Reynolds shear stress, skewness factor, flatness factor

1. INTRODUCTION

Gas injection techniques have been utilized widely in a variety of engineering fields. In most cases, gas is injected into a bath through a bottom nozzle or a bottom orifice (bottom injection), and hence, the direction of the inertia force of injected gas is the same as that of the buoyancy force of bubbles generated in the bath. Many investigations have been carried out on the bubble formation from a nozzle or an orifice, rising bubble behavior, and liquid motion induced by rising bubbles (Davidson and Amick 1956; Tadaki and Maeda 1963; Kumar and Kuloor 1970; Irons and Guthrie 1978; Hoefele and Brimacombe 1979; Ozawa and Mori 1982; Iguchi *et al.* 1992, 1994, 1995a–c, 1997).

In practical situations, however, we often encounter the case that the direction of the inertia force of injected fluid is opposite to the direction of the buoyancy force of bubbles. Such top injections can be classified further into two categories: top gas injection and top liquid injection. The former injection has been utilized in steelmaking processes extensively (ISIJ 1984; Sahai and Pierre, 1992), while the latter injection, the jet being called a plunging jet, has been utilized mainly in chemical engineering (see a recent review article by Bin 1993).

Although a lot of studies have been carried out for the two types of top injections, previous investigators have mentioned primarily on the behavior of bubbles. Little is known about turbulent liquid motion in the bubble dispersion region (McKeogh and Ervine 1981; Bonetto and Lahey 1993). The main purpose of this study is to investigate the behavior of bubbles and liquid flow motion induced by a plunging jet.

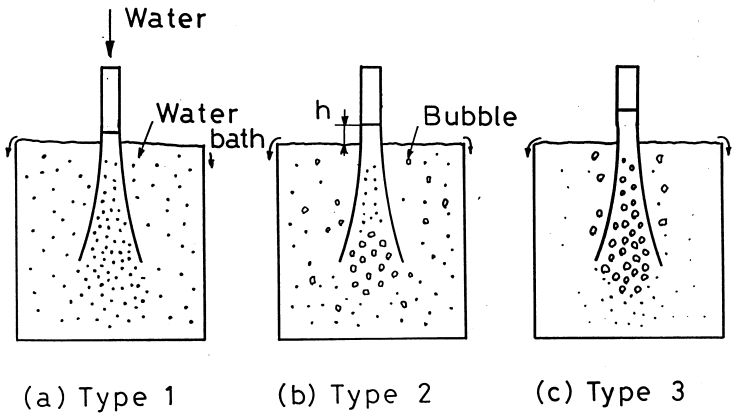

Figure 1. Three types of bubble dispersion patterns.

McKeogh and Ervine (1981) and Shakouchi *et al.* (1995, 1996) have treated the same flow field as mentioned here and reported that there exist three types of bubble dispersion patterns in the case that the plunging water jet impacts the bath surface before its breakup, as shown schematically in figure 1. When the distance from the pipe exit to the undisturbed bath surface is short, and accordingly, the surface of the water jet is smooth, a lot of small bubbles are generated and they disperse in the whole bath (type 1). On the other hand, when the distance is long and the surface of the water jet is rough, relatively large bubbles are generated and the bubble dispersion region is localized beneath the pipe exit (type 3). The bubble dispersion patterns of types 1 and 3 appear simultaneously for an intermediate distance (type 2). Exact knowledge about the boundaries among these three regimes, however, are not obtained.

Bubble entrainment may be closely related to the shear flow instability on the plunging jet surface. This subject is, however, beyond the scope of the present work, and the boundaries are determined by observing bubble dispersion patterns in the bath.

The main purpose of this study is to present detailed data on the mean and turbulence characteristics in bubbly flows induced by a plunging water jet in a water bath. The information on these characteristics would be useful for understanding the mixing condition in the bath as well as for developing new turbulence models for bubbly flows.

We measured the mean velocity and turbulence components of water flow in the bubble dispersion region of types 1 and 3 using a two-channel LDV system and compared the results with those for single-phase free jets and vertical bubbling jets induced by bottom gas injection.

2. EXPERIMENTAL APPARATUS AND MEASUREMENT METHOD

Figure 2 shows a schematic of the experimental apparatus. The dimensions of the experimental apparatus were determined by referring to McKeogh and Ervine (1981), Bonetto and Lahey (1993), and Shakouchi *et al.* (1995, 1996). The vessel made of transparent acrylic resin had an inner diameter D of 20.0 cm and a height H of 39.0 cm. The origin of the cylindrical coordinate system was placed on the undisturbed bath surface. The axial and radial coordinates were denoted by z and r, respectively. The corresponding velocity components were designated by u and v. Water was injected through a straight circular pipe of an inner diameter d of 0.5 cm and a length L of 60 cm into a water bath. The plunging water jet thus generated impacted a pool of water at 90°.

Experimental conditions were also determined by consulting with the previous investigators (McKeogh and Ervine 1981; Bonetto and Lahey 1993; Shakouchi *et al.* 1995, 1996). The plunging water jet flow-rate Q_w was changed from 50 cm^3/s to 66.7 cm^3/s and the corresponding mean velocity at the pipe exit $\bar{u}_0$ $[=4Q_w/(\pi d^2)]$ ranged from 254 cm/s to 340 cm/s. The pipe Reynolds number was higher than 1×10^4 and the aspect ratio L/d was 120. Accordingly, the water flow in the pipe was turbulent and fully developed at the pipe exit. The turbulence intensity at the pipe exit increased monotonically from approximately 5% in the central part to ap-

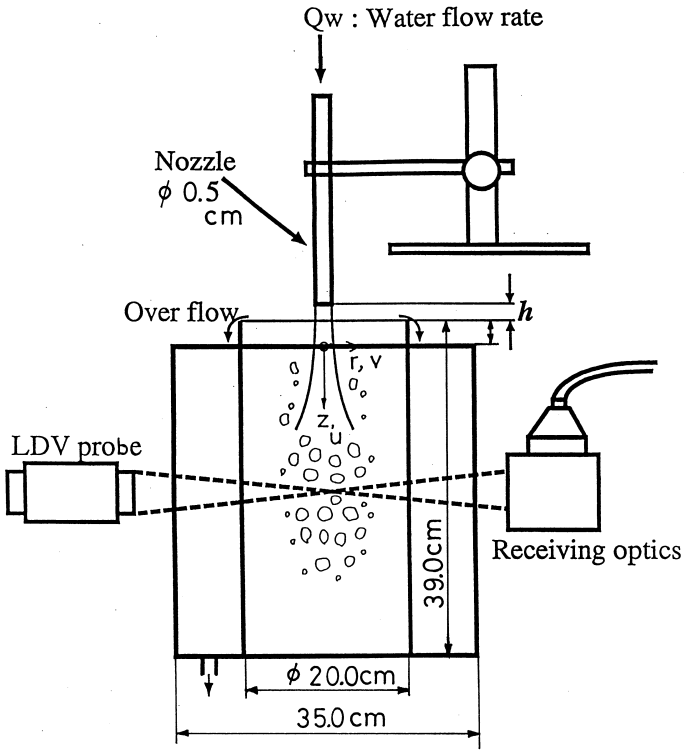

Figure 2. Experimental apparatus.

proximately 15% in the outer part of the pipe flow. These turbulence intensity data were described here because the turbulence intensity in nozzles and pipes used for producing a plunging water jet is known to affect the behavior of bubbles significantly (Bin 1993).

The distance from the pipe exit to the undisturbed bath surface, h, was set at 0.2 or 1 cm. The bubble dispersion patterns of types 1 and 3 appeared for $h = 0.2$ and 1.0 cm, respectively, as shown in figure 3. Three kinds of symbols (○, ▲, □) represent types 1 ∽ 3 observed by Shakouchi *et al.* (1995, 1996).

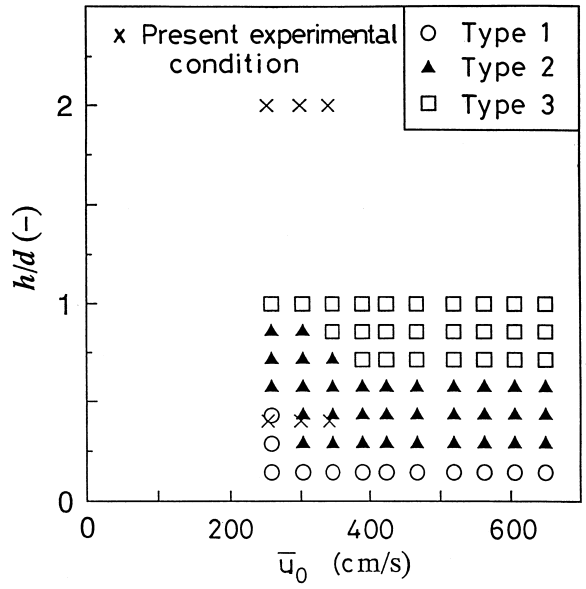

Figure 3. The limits between three bubble dispersion patterns and the present experimental conditions.

Although the threshold value of the mean jet velocity $\bar{u}_{0e}$ at which gas entrainment commences is far more ambiguous for turbulent plunging jets, rough estimation for the droplet region can be given by (Bin 1993)

$$\bar{u}_{0e} = 5h^{0.534} \quad [1]$$

The units of $\bar{u}_{0e}$ and h are m/s and m, respectively. Equation [1] is valid for $h = 0.015$–0.40 m. The average error in predicting $\bar{u}_{0e}$ from [1] is $\pm 8\%$.

Equation [1] yields $\bar{u}_e = 18$ cm/s and 43 cm/s for $h = 0.2$ and 1.0 cm, respectively. On the other hand, $\bar{u}_{0e}$ is 80 cm/s both for types 1 and 3 in the continuous jet region (see figure 8 in Bin 1993). Anyway, these $\bar{u}_{0e}$ values are much smaller than the minimum nozzle exit velocity $\bar{u}_0$ of 254 cm/s chosen in this study. These results suggest that bubbles are entrained in the water bath under every experimental condition investigated in this study. This was confirmed from experiments.

The dispersion of bubbles in the bath was observed using a camera and by naked eye inspection. The axial and radial velocity components, u and v, were measured with a two-channel laser Doppler velocimeter (LDV) except in the close vicinity of the bath surface ($z < 8$ cm). Reliable velocity measurements could not be made there due to the existence of so many small bubbles. The adequacy of LDV measurements for $z > 8$ cm were judged by referring to the previous article (Iguchi *et al.* 1994). The uncertainty of velocity measurements in this axial region is $\pm 3\%$. Concerning LDV measurements in the close vicinity of the bath surface, a recent article by Bonetto and Lahey (1993) should be referred.

Velocity data were decomposed into the mean velocity and turbulence components as follows:

$$\bar{u} = \Sigma u_i / N \quad [2]$$

$$\bar{v} = \Sigma v_i / N \quad [3]$$

$$u_i' = u_i - \bar{u} \quad [4]$$

$$v_i' = v_i - \bar{v} \quad [5]$$

where N is the total number of sampling data and the subscript i designates the ith digitized datum.

3. EXPERIMENTAL RESULTS AND DISCUSSION

3.1. *Bubble behavior*

Bubbles taken by a camera for types 1 and 3 were shown in figure 4. The diameter of bubbles generated at the bath surface for type 1 was less than 0.1 cm but the maximum diameter became approximately 0.15 cm near the bottom wall (30 cm $\lesssim z \leqq$ 39 cm) due to the coalescence of small bubbles. The bubbles rose along the side wall and escaped from the bath surface. The diameter of bubbles for type 3 attained up to approximately 0.4 cm. These large bubbles were localized beneath the pipe exit, while very small bubbles much less than 0.1 cm in diameter arrived near the bottom wall and rose along the side wall.

According to Bin (1993), the penetration depth of bubbles, H_p (m), can be expressed by

$$H_p = 0.42 \bar{u}_{Bs}^{4/3} d_{Bs} Q_G^{-1/4} \quad [6]$$

where $\bar{u}_{Bs}$ (m/s) is the mean water jet velocity at the bath surface and d_{Bs} (m) is the jet diameter at the bath surface, and Q_G (m^3/s) is the entrained air flow-rate. The mean velocity $\bar{u}_{Bs}$ can be calculated as $(\bar{u}_0^2 + 2gh)^{1/2}$ and the air flow-rate can be estimated from an equation described in a later section.

Equation [6] can approximate experimental data obtained with nozzles of diameter ranging from 3.9 to 12 mm and for $h < 0.50$ m within a scatter of $\pm 20\%$.

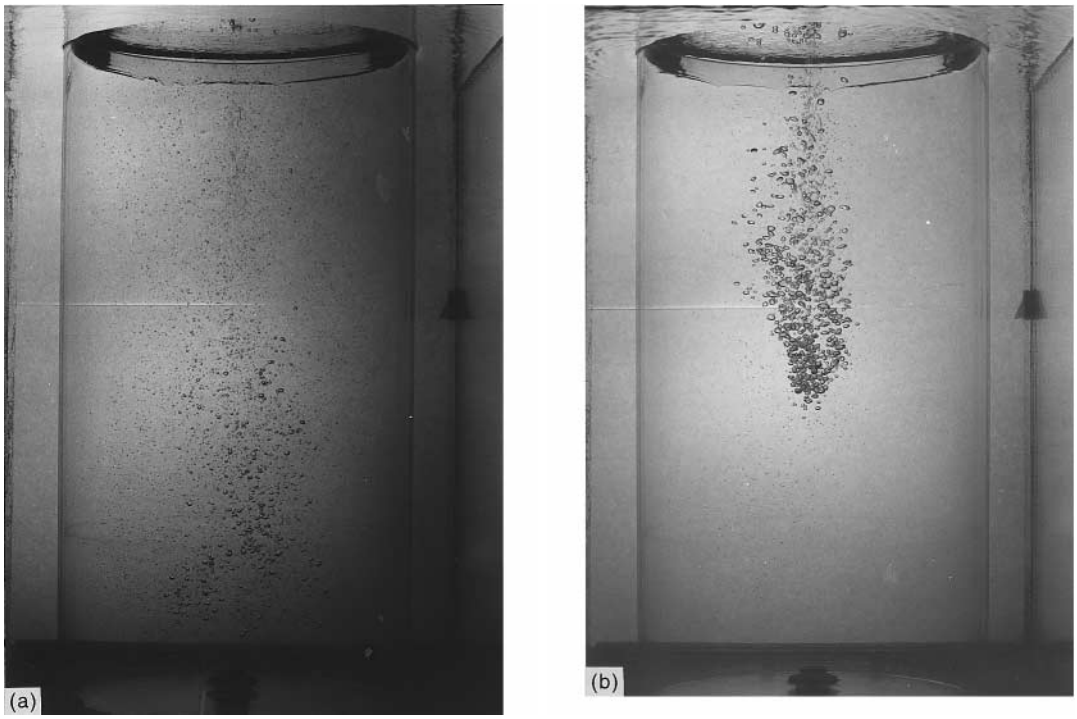

Figure 4. Photographs showing bubble dispersion patterns typical of types 1 and 3 ($Q_w = 50\ cm^3/s$).

If we assume $\bar{u}_{Bs} \doteqdot \bar{u}_0$ and $d_{Bs} \doteqdot d$, [6] can be rewritten by

$$H_p = 0.42 \bar{u}_0^{4/3} d Q_G^{-1/4} \quad [7]$$

Equation [7] yields $H_p = 15.3$ cm for $h = 0.2$ cm and $H_p = 13.1$ cm for $h = 1.0$ cm. The presently observed H_p value was larger than 30 cm for $h = 0.2$ cm and $H_p = 23$ cm for large bubbles for $h = 1.0$ cm. The difference between the presently observed and calculated H_p values for each type may be attributable to the low accuracy of the evaluation of d_{Bs}. The evaluation of the adequacy of [7] should be left for a future study.

3.2. *Distributions of the axial mean velocity and turbulence components on the centerline of bubble dispersion region*

3.2.1. *Mean velocity component*. Data on the axial mean velocity on the centerline of the plunging jet, $\bar{u}_{c1}$, obtained for $h = 0.2$ cm were plotted against the axial distance z in figure 5. The measured $\bar{u}_{c1}$ values for a water flow-rate of $Q_w = 50\ cm^3/s$ (type 1) can be approximated satisfactorily by the following empirical equation for single-phase free jets (Ishigaki 1982; Iguchi *et al.* 1989).

$$\bar{u}_{c1}/\bar{u}_0 = 6.2 d/z \quad [8]$$

where $\bar{u}_0$ is the mean velocity of water at the pipe exit and d is the inner pipe diameter. Equation [8] is known to be valid for $z/d \gtrsim 10$. Single-phase free jet means a jet issuing from a nozzle into an infinite space occupied by the same fluid as the jet. Such good agreement means that the axial mean velocity $\bar{u}_{c1}$ is not affected by bubbles in diameter smaller than approximately 0.1 cm, which are entrained from the bath surface around the water jet, because they are too small to interact with the plunging water jet.

The measured $\bar{u}_{c1}$ values for $Q_w = 66.7\ cm^3/s$ (type 2) were also predicted by [8] because this water flow-rate fell near the limit between types 1 and 2, as shown in figure 3.

Measured $\bar{u}_{c1}$ values for $h = 1.0$ cm and $Q_w = 50\ cm^3/s$ were compared with those for $h = 0.2$ cm and $Q_w = 50\ cm^3/s$ in figure 6. In the axial region of $z \gtrsim 15$ cm, [8] could not predict the measured values for $h = 1.0$ cm any more. This reason is explained as follows: The maximum bubble diameter for $h = 1.0$ cm is much larger than that for $h = 0.2$ cm, and the buoy-

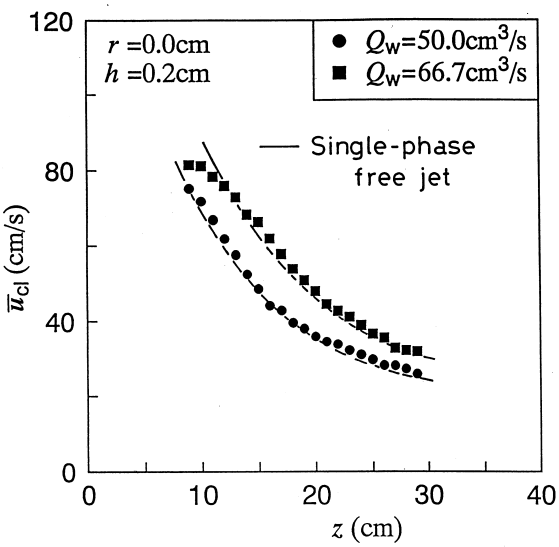

Figure 5. Relation between the axial mean velocity on the centerline and axial distance z.

ancy force of bubbles plays a more important role for $h = 1.0$ cm than for $h = 0.2$ cm. As a result, the downward water motion for type 3 was highly suppressed for $z \gtrsim 15$ cm.

McKeogh and Ervine measured $\bar{u}_{c1}$ with a Pitot tube and derived the following relation for $z/d > 3$.

$$\bar{u}_{c1}/\bar{u}_0 = 3.3(d/z)^{1.1} \tag{9}$$

Equation [9] does not agree with the presently measured values for type 1, but for type 3 this equation makes almost good agreement with the measured values at $z \gtrsim 20$ cm. This limit value of 20 cm gives $z/d = 40$, thus being different significantly from $z/d = 3$ proposed by McKeogh and Ervine.

Although McKeogh and Ervine used a Pitot tube, this tube is said to be unable to detect the liquid-phase velocity in the bubble dispersion region precisely (Bin, 1993). Another reason may cause the disagreement between the present measured values and [9] for $z/d \lesssim 40$. More data on $\bar{u}_{c1}$ should be accumulated to discuss the validity of [9].

According to the previous experimental results for an upward premixed water and air injection (Iguchi *et al.*, 1997), the half-value radius, b_u, of the axial mean velocity component $\bar{u}$ can be expressed by the following equation in the presence of turbulence production in the wake of bubbles.

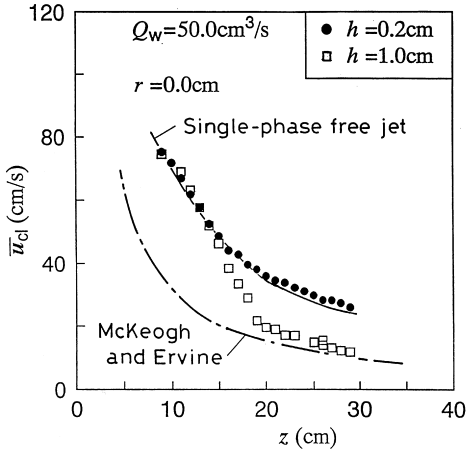

Figure 6. Relation between the axial mean velocity on the centerline and axial distance z for different distances from the pipe exit and the bath surface.

$$b_u = [2ln2]^{1/2} Cz \quad [10]$$

$$C = 0.046\varepsilon' + 0.071 \quad [11]$$

$$\varepsilon' = Q_G/(Q_G + Q_w) \quad [12]$$

Equation [10] is valid for $z/d \gtrsim 10$ and $0 \leqq \varepsilon' \leqq 1$.

The coefficient C is 0.071 for water jets generated by bottom water injection and $C = 0.117$ for bubbling jets generated by bottom gas injection. Also, C is 0.071 for a single-phase free jet. Gas-liquid two-phase jets, therefore, spread wider in the transverse direction than single-phase free jets.

In order to examine the validity of [10] for types 1 and 3, C should be evaluated. The following relation was derived for the entrained gas flow-rate Q_G by Bin (1993)

$$Q_G = 0.04 Q_w Fr^{0.28} (h/d)^{0.4} \quad [13]$$

$$Fr = \bar{u}_0^2/(gd) \quad [14]$$

where Fr is the Froude number. Equation [13] is valid for $h/d \leqq 100$, $L/d \geqq 10$ and $Fr^{0.28}(h/d)^{0.4} \geqq 10$ within an uncertainty of $\pm 20\%$.

For type 3, substitution of $\bar{u}_0 = 254$ cm/s, $Q_w = 50$ cm^3/s, $d = 0.5$ cm and $h = 1.0$ cm into [13] and [14] yields

$$Q_G = 10.4\,\text{cm}^3/\text{s} \quad [15]$$

Combination of [10]–[12] and [15] gives

$$C = 0.079 \quad [16]$$

$$b_u = 0.093z \quad [17]$$

Equation [17], drawn by a dot-dash line in figure 7, is in almost good agreement with the measured values at $z = 10$ cm although the directions of the inertia force of plunging water jet and the buoyancy force of bubbles are opposite. As z increases, the deviation of the measured values from [17] increases. This means that the buoyancy effect is so small as to be neglected near the nozzle but become significant away from the nozzle.

On the other hand, for type 1, the following empirical equation for single-phase free jets is a good approximation at $z = 10$ and 20 cm

$$b_u = 0.084z \quad [18]$$

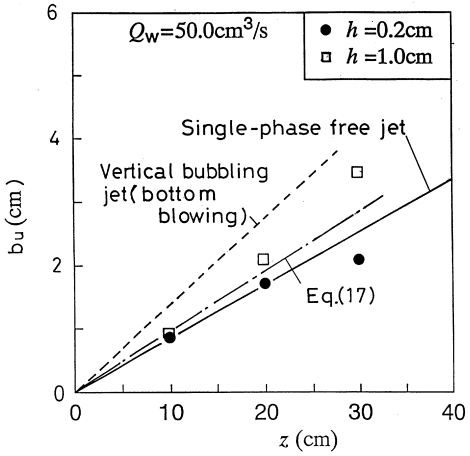

Figure 7. Relation between the half-value radius b_u and axial distance z.

The flow at $z = 30$ cm is considered to be affected by a vortex motion induced by the bottom wall and the side wall, and hence, [18] overestimates the b_u value.

Meanwhile, [13] yields $Q_G = 5.4\ \mathrm{cm}^3/\mathrm{s}$ for type 1 and then [10] gives

$$b_u = 0.088z \qquad [19]$$

This [19], however, is not applicable to type 1 because [10] was derived originally in the presence of the turbulence production in the wake of bubbles.

In figure 6, the $\bar{u}_{c1}$ value for type 1 ($h = 0.2$ cm) has small influence of flow direction. However, the half-value radius b_u at $z = 30$ cm has large influence. This is probably due to the existence of the above-mentioned vortex motion near the bottom wall.

3.2.2. *The root-mean-square (rms) values of turbulence components.* The rms values of the axial and radial turbulence components, u'_{rms} and v'_{rms}, are defined by

$$u'_{rms} = [\Sigma u_i'^2/N]^{1/2} \qquad [20]$$

$$v'_{rms} = [\Sigma v_i'^2/N]^{1/2} \qquad [21]$$

Measured values of u'_{rms} on the centerline, denoted by $u'_{rms,cl}$, were plotted in figure 8. For each water flow-rate, the measured values for type 1 were larger than those for type 3 in the axial region of $z \gtrsim 15$ cm. This 15 cm is smaller than the penetration depth of bubbles, H_p. Consequently, the turbulence production was also suppressed due to the localization effect of bubbles beneath the pipe exit. The reason is explained as follows:

Turbulence production in the wake of bubbles takes place for type 3, while another turbulence production due to the entrainment of surrounding water into the jet is lowered significantly because $\bar{u}_{c1}$ decreases to a great extent, as shown in figure 6.

The ratio of $u'_{rms,cl}$ to $\bar{u}_{c1}$ was defined as the turbulence intensity on the centerline and designated by $T_{u,c1}$. Measured $T_{u,c1}$ values for type 1 agreed approximately with a single-phase free jet value of around 0.3 (Wygnanski and Fiedler 1969), as shown in figure 9, implying that turbulence production was hardly affected by small bubbles.

The measured $T_{u,c1}$ values for type 3 did not agree with the single-phase free jet value in the axial region of $z \gtrsim 15$ cm. The axial $T_{u,c1}$ distribution exhibits a peak, and with a further increase in z, $T_{u,c1}$ seems to approach a constant value. Bonetto and Lahey (1993) also observed that the liquid flow field for type 1 is practically unaffected by bubbles, while in the case of type 3 the bubbles are much larger, thus the dispersed phase (bubbles) increases the continuous phase turbulence intensity.

However, clear explanation for these phenomena has not been given by Bonetto and Lahey (1993). An attempt to explain these phenomena will be made subsequently.

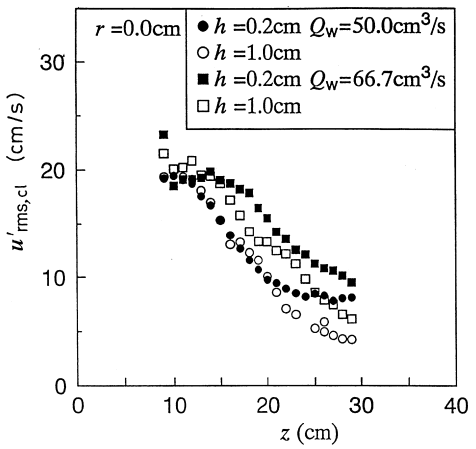

Figure 8. Relation between the rms value of the axial turbulence component on the centerline and axial distance z.

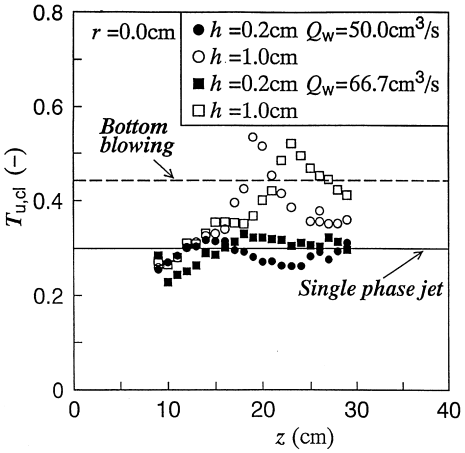

Figure 9. Turbulence intensity on the centerline.

The bubble Reynolds number Re_B is defined by

$$Re_B = | \bar{u}_B - \bar{u} | \bar{d}_B / \nu \quad [22]$$

where $\bar{u}_B$ is the mean bubble velocity, $\bar{u}$ is the axial mean velocity of water, and ν is the kinematic viscosity of water. According to the previous experiments for upward bubbling jets (Iguchi *et al.* 1995a,b, 1997), $|\bar{u}_B - \bar{u}|$ is estimated to be approximately 20 cm/s in its maximum value for small bubbles with diameter less than 0.1 cm. This fact suggests that for type 1, small bubbles with $\bar{u}_B < 0.1$ cm, conveyed deep in the bath by water jet, also move with a relative velocity $|\bar{u}_B - \bar{u}|$ of less than 20 cm/s, and hence, $Re_B < 200$.

Since the wake of bubbles undergoes transition to turbulence for $Re_B \gtrsim 400$ (Hetsroni 1989), the wake of bubbles is laminar for type 1 and additional turbulence is not produced. This is the main reason for the agreement between the presently measured $T_{u,c1}$ values and the single-phase free jet value.

The bubble Reynolds number Re_B for type 3 was approximately 800 in its highest value [$\bar{d}_B \fallingdotseq 0.4$ cm, $|\bar{u}_B - \bar{u}| \fallingdotseq 20$ cm/s because large bubbles of $\bar{d}_B \fallingdotseq 0.4$ cm were almost at rest ($\bar{u}_B \fallingdotseq 0$) and $\bar{u} \fallingdotseq 20$ cm/s in an axial region of $z \fallingdotseq 20$–30 cm, as shown in figure 6]. Consequently, turbulence was produced in the wake of bubbles. Such additional turbulence production is associated with the peak in the $T_{u,c1}$ distribution. The decrease in $T_{u,c1}$ with a further increase in z is related to the cessation of turbulence production in the wake of bubbles. Bubbles with diameters enough to generate turbulence in their wake can not penetrate there.

The axial position, at which the peak value of $T_{u,c1}$ was taken, shifted downward as the water flow-rate increased. This is closely related to an increase in the bubble penetration depth due to an increase in the inertia force of injected water (Bin, 1993). The height of the peak, $T_{u,c1} \fallingdotseq 0.55$, was independent of the water flow-rate and larger than the value, $T_{u,c1} \fallingdotseq 0.45$, reported for a vertical bubbling jet generated in a water bath agitated by bottom gas injection.

3.3. *Radial distributions of mean velocity and turbulence components*

3.3.1. *Mean velocity component.* Measurements of the radial distributions of $\bar{u}$ were carried out at three representative axial positions of z = 10, 20, and 30 cm for two h values of 0.2 and 1.0 cm. The axial mean velocity $\bar{u}$ was non-dimensionalized by its centerline value, $\bar{u}_{c1}$, and plotted against the non-dimensionalized radial distance r/b_u in figure 10. Here b_u is the half-value radius of the radial $\bar{u}$ distribution. In the central part of the bubble dispersion region ($r/b_u \lesssim 2$), all the measured values were able to be approximated by a Gaussian distribution indicated by a solid line, as suggested by McKeogh and Ervine (1981). The $\bar{u}/\bar{u}_{c1}$ values became negative as r/b_u increased further due to upward moving motion of water.

Such an agreement between the measured $\bar{u}/\bar{u}_{c1}$ values and a Gaussian distribution for $r/b_u \lesssim 2$ was also observed for vertical bubbling jets generated by injecting gas through a single-hole bottom nozzle or a single-hole bottom orifice into a water bath (Iguchi *et al.* 1995b). In addition,

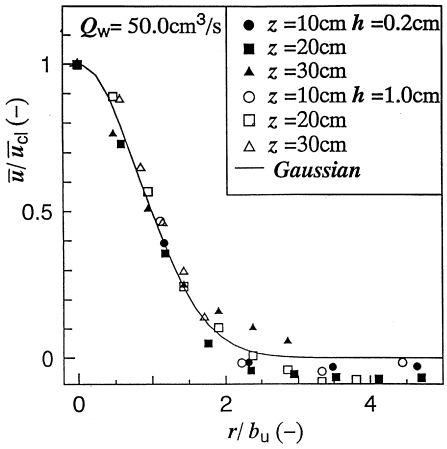

Figure 10. Radial distributions of the axial mean velocity.

the same tendency was reported for vertical bubbling jets generated by injecting a premixed gas and water through a single-hole bottom nozzle into a water bath (Iguchi *et al.* 1997).

The present experimental results mean that the effect of bubble size on the radial $\bar{u}/\bar{u}_{c1}$ distribution is not significant in the central part of the bubble dispersion region ($r/b_u \lesssim 2$). The same was true for $Q_w = 66.7$ cm^3/s though the evidence was not given in this article.

3.3.2. *Radial distributions of the axial and radial turbulence components*. The rms values of the axial and radial turbulence components, and v'_{rms}, were divided by the centerline value of the axial mean velocity, $\bar{u}_{c1}$, and shown in figures 11 and 12, respectively. The shaded and open symbols denote the axial and radial turbulence components, respectively. The solid and broken lines indicate the distributions of u'_{rms} and v'_{rms}reported by Wygnanski and Fiedler (1969) for single-phase free jets.

As expected from figure 9, the measured values of the axial and radial turbulence components at z = 10 cm and 20 cm, shown in figure 11, agreed approximately with their respective single-phase jet values in the central part of the bubble dispersion region ($r/b_u \lesssim 2$). However, in the outer region ($r/b_u \gtrsim 2$), the measured values of the two turbulence components agreed with each other and never diminished. This is just the same as reported for a bubbling jet in a water bath agitated by bottom gas injection (Iguchi *et al.*, 1995b). The $u'_{rms,cl} >$ values for $r/b_u \lesssim 2$ at z = 30 cm are larger than the single-phase jet values through the effect of the bottom wall.

In figure 12 agreement between the measured values of the two turbulence components for $r/b_u \lesssim 2$ and their respective single-phase jet values was good only at z = 10 cm. This is because the relative velocity between bubbles and water is small at this axial position, and accordingly,

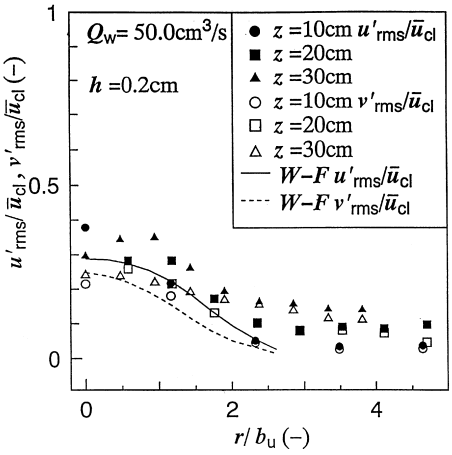

Figure 11. Radial distributions of the rms values of the axial and radial turbulence components for h = 0.2 cm.

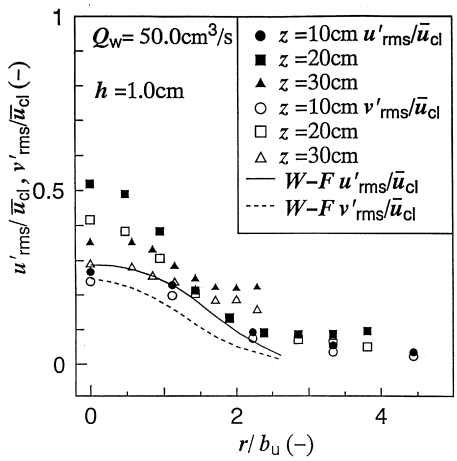

Figure 12. Radial distributions of the rms values of the axial and radial turbulence components for $h = 1.0$ cm.

turbulence production in the wake of bubbles does not take place. Meanwhile, the measured values of the two turbulence components were much larger than their respective single-phase jet values at $z = 20$ cm. This difference is attributable to additional turbulence production in the wake of bubbles, as discussed in the preceding section. Also in this case, the $u'_{rms}/\bar{u}_{cl}$ values at $z = 30$ cm are larger than the single-phase jet value because of the convection of turbulent eddies generated upstream as well as the bottom wall effect.

3.3.3. *Radial distributions of Reynolds shear stress*. The Reynolds shear stress can be calculated from

$$\overline{u'v'} = \Sigma u'_i v'_i / N \qquad [23]$$

Recently, the mean velocity and the rms values of the turbulence components mentioned above have been measured by Bonetto and Lahey (1993) in the close vicinity of the bath surface. The Reynolds shear stress and higher turbulence correlations such as skewness and flatness factors, however, have not been considered although these quantities are useful for revealing the turbulence structure of bubbly flows and mixing in the bath. The information on the turbulence structure is necessary for developing turbulence models for gas-liquid two-phase flows, too.

Measured values of the non-dimensionalized Reynolds shear stress, $\overline{u'v'}/\bar{u}_{c1}^2$, for $h = 0.2$ cm and 1.0 cm were shown in figures 13 and 14, respectively. In figure 13, the Reynolds shear stress values measured at $z = 10$ and 20 cm are in almost good agreement with single-phase free jet values obtained by Wygnanski and Fiedler (1969), while those for $z = 30$ cm are much higher than the single-phase jet value. This fact means that the Reynolds shear stress at $z = 30$ cm

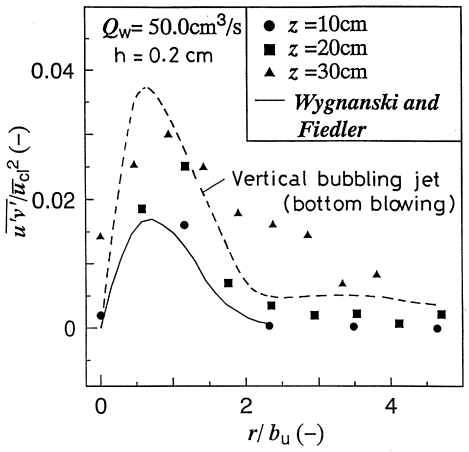

Figure 13. Radial distributions of the Reynolds shear stress for $h = 0.2$ cm.

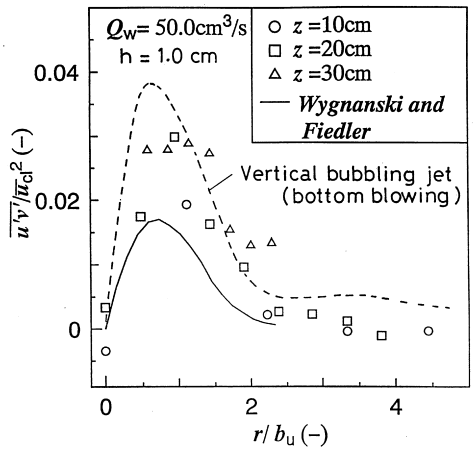

Figure 14. Radial distributions of the Reynolds shear stress for h = 1.0 cm.

(9 cm above the bottom wall) is more sensitive to the existence of the bottom wall than u'_{rms} and v'_{rms}.

For h = 1.0 cm the measured $\overline{u'v'}/\bar{u}_{c1}^2$ values agreed approximately with the single-phase jet value at z = 10 cm but those at z = 20 and 30 cm were much larger than the single-phase jet value, as shown in figure 14. These results are in accordance with the measured radial distributions of the axial and radial turbulence components. The measured $\overline{u'v'}/\bar{u}_{c1}^2$ values at z = 20 and 30 cm did not agree with the broken line for a vertical bubbling jet.

3.3.4. *Skewness and flatness factors.* Skewness factors, S_u and S_v and flatness factors, F_u and F_v, are commonly used to describe the probability distribution functions of the axial and radial turbulence components u' and v'. These factors are defined by

$$S_u = [\Sigma u_i'^3/N]/u'^3_{rms} \quad [24]$$

$$S_v = [\Sigma v_i'^3/N]/v'^3_{rms} \quad [25]$$

$$F_u = [\Sigma u_i'^4/N]/u'^4_{rms} \quad [26]$$

$$F_v = [\Sigma u_i'^4/N]/u'^4_{rms} \quad [27]$$

The physical meaning of these factors should be referred to the previous articles (Iguchi *et al.* 1995b, 1997).

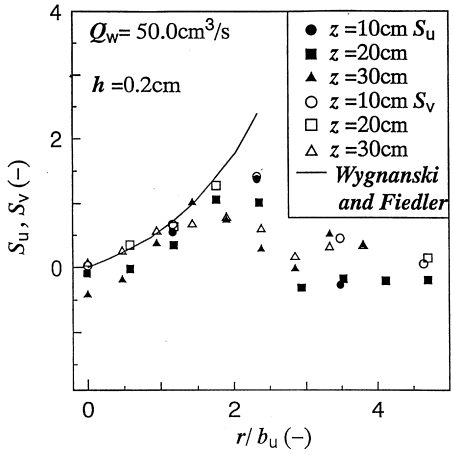

Figure 15. Radial distributions of the skewness factor for h = 0.2 cm.

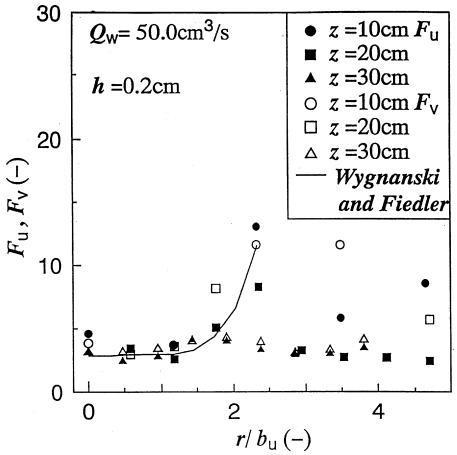

Figure 16. Radial distributions of the flatness factor for $h = 0.2$ cm.

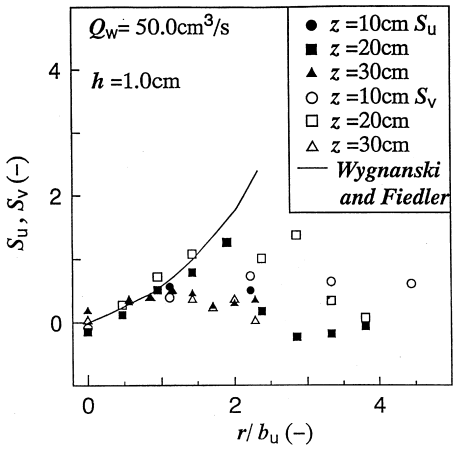

Figure 17. Radial distributions of the skewness factor for $h = 1.0$ cm.

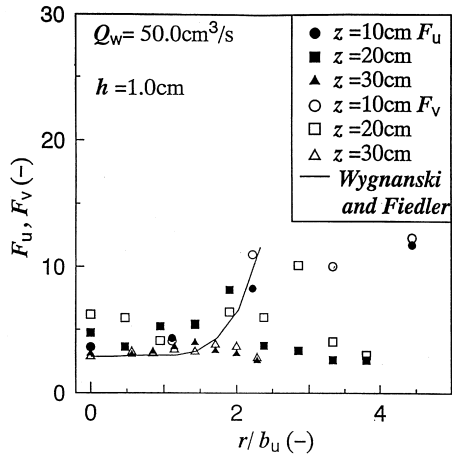

Figure 18. Radial distributions of the flatness factor for $h = 1.0$ cm.

Measured values of the skewness and flatness factors for $h = 0.2$ cm were shown in figures 15 and 16, respectively. In the central part of the bubble dispersion region ($r/b_u \lesssim 2$), all the measured values are compared satisfactorily with the single-phase jet values except for S_u at $z = 30$ cm. These results are almost consistent with the results of the rms values of the two turbulence components (figure 11) and the Reynolds shear stress (figure 13). In the outer region ($r/b_u \gtrsim 2$), definite trend cannot be seen.

Figures 17 and 18 show measured values of the skewness and flatness factors for $h = 1.0$ cm, respectively. In the central part of the bubble dispersion region ($r/b_u \lesssim 2$), the measured values of S_u, S_v, F_u, and F_v at $z = 10$ and 30 cm are in good agreement with their respective single-phase jet values. This is because additional turbulence production in the wake of bubbles does not occur at these two axial positions ($Re_B < 400$ at $z = 10$ and 30 cm). The measured S_u, S_v, F_u, and F_v values at $z = 20$ cm, however, changed in the radial direction in a complex manner. More data should be accumulated to derive definite conclusions on the skewness and flatness factors for type 3.

4. CONCLUDING REMARKS

Water was injected vertically downward onto a water bath through a circular pipe. Entrained air was disintegrated into bubbles as they passed through the bath surface. Bubble dispersion patterns were classified into three types with respect to the distance from the pipe exit to the undisturbed bath surface, h. Small bubbles ($d_B \lesssim 0.1$ cm) were generated for a small h value and they spread in the whole bath (type 1). Relatively large bubbles ($d_B \lesssim 0.4$ cm) were generated for a large h value and they were localized beneath the pipe exit (type 3).

Table 1 was given for better understanding of the present experimental results. In the case of type 1, the mean velocity and turbulence characteristics in the central part of the bubble dispersion region were approximated satisfactorily by empirical correlations originally proposed for single-phase free jets except near the bottom wall ($30 \lesssim z \leqq 39$ cm). Consequently, small bubbles with diameters less than 0.1 cm hardly affected the motion of water in the bubble dispersion region. This is because the bubble Reynolds number Re_B was less than 400, and the wake of bubbles does not undergo to turbulence transition.

The maximum bubble diameter for type 3 was approximately 0.4 cm, and the maximum bubble Reynolds number was estimated to be 800. The axial mean velocity component $\bar{u}$ and the turbulence components in the bubble dispersion region were affected significantly by bubbles except near the bath surface ($z = 10$ cm). This is closely associated with additional turbulence production in the wake of bubbles, as reported previously for a bubbling jet caused by bottom gas injection. However, the turbulence characteristics of water flow investigated here were not predicted from the information on the bubbling jet generated by bottom gas injection.

Table 1. Summary of the axial and radial mean velocity and turbulence characteristics in the bubble dispersion region ($r/b_u \lesssim 2$)

		Axial characteristics				Radial characteristics								
Type	z(cm)	$\bar{u}_{c1}$	b_u	$u'_{rms,c1}$	$T_{u,c1}$	$\bar{u}/\bar{u}_{c1}$	$u'_{rms}/\bar{u}_{c1}$	$v'_{rms}/\bar{u}_{c1}$	$u'v'/\bar{u}_{c1}^2$	S_u	S_v	F_u	F_v	Remarks
						$\bar{u}_{c1}$	$\bar{u}_{c1}$	$\bar{u}_{c1}$	$\bar{u}_{c1}^2$					
	10	○	○	○	○	○	○	○	○	○	○	○	○	†
1	20	○	○	○	○	○	○	○	○	○	○	○	○	†
	30	○	◑	○	○	○	◑	◑	●	●	○	○	○	†,‡
	10	○	○	○	○	○	○	○	○	○	○	○	○	†
3	20	●	●	●	●	○	●	●	●	●	●	●	●	§
	30	●	●	●	●	○	◑	◑	●	○	○	○	○	†,‡,¶

○ Agreement with single-phase free jet value; ◑ Indefinite; ● Disagreement with single-phase free jet value.
† No turbulence production in the wake of bubbles.
‡ Bottom wall effect.
§ Turbulence production in the wake of bubbles.
¶ Convection of turbulence eddies generated upstream

Quantitative correlation of the mean velocity and turbulence characteristics for type 3 should be left for a future study.

REFERENCES

Bin, A. K. (1993) Gas entrainment by plunging liquid jets. *Chem. Eng. Sci.* **48,** 3585–3630.

Bonetto, F. and Lahey, R. T. Jr (1993) An experimental study on air carryunder due to a plunging liquid jet. *Int. J. Multiphase Flow* **19,** 281–294.

Davidson, L. and Amick, E. H. Jr (1956) Formation of gas bubbles at horizontal orifices. *AIChE J.* **2,** 337–342.

Hetsroni, G. (1989) Particle–turbulence interaction. *Int. J. Multiphase Flow* **15,** 735–746.

Hoefele, E. O. and Brimacombe, J. K. (1979) Flow regimes in submerged gas injection. *Met. Trans.* **10B,** 631–648.

Iguchi, M., Tani, J., Uemura, T., Kawabata, H., Takeuchi, H. and Morita Z. (1989) The characteristics of water and bubbling jets in a cylindrical vessel with bottom blowing. *ISIJ Int.* **29**, 309–317.

Iguchi, M., Demoto, Y., Sugawara, N. and Morita, Z. (1992) Behavior of Hg–air vertical bubbling jets in a cylindrical vessel. *ISIJ Int.* **32,** 998–1005.

Iguchi, M., Kondoh, T. and Uemura, T. (1994) Simultaneous measurement of liquid and bubble velocities in a cylindrical bath subject to centric bottom gas injection. *Int. J. Multiphase Flow* **20,** 753–762.

Iguchi, M., Kawabata, H., Nakajima, K. and Morita, Z. (1995a) Measurement of bubble characteristics in a molten iron bath at 1600°C using an electroresistivity probe. *Metal. Mater. Trans. B* **26**, 67–74.

Iguchi, M., Ueda, H. and Uemura, T. (1995b) Bubble and liquid flow characteristics in a vertical bubbling jet. *Int. J. Multiphase Flow* **21,** 861–873.

Iguchi, M., Takanashi, N., Ogawa, Y., Tokumitsu, N. and Morita, Z. (1995c) X-ray fluoroscopic observation of bubble characteristics in a molten iron bath. *ISIJ Int.* **35,** 515–520.

Iguchi, M., Okita, K., Nakatani, T. and Kasai, N. (1997) Structure of turbulent round bubbling jet generated by premixed gas and liquid injection. *Int. J. Multiphase Flow* **23,** 249–262.

Iron Steel Inst. Jpn. (1984) Recent development in materials refining processes agitated by gas injection. *Nishiyama Memorial Lecture Series*. 101/102, Iron Steel Inst. Jpn. (in Japanese) .

Irons, G. A. and Guthrie, R. I. L. (1978) Bubble formation at nozzles in pig iron. *Met. Trans.* **9B,** 101–110.

Ishigaki, H. (1982) Turbulent round jets. *Trans. Jpn. Soc. Mech. Eng.* **49**, 1692–1700 (in Japanese) .

Kumar, R. and Kuloor, N. R. (1970) The formation of bubbles and drops. *Adv. In Chem. Eng.* **8,** 255–369.

McKeogh, E. J. and Ervine, D. A. (1981) Air entrainment rate and diffusion pattern of plunging liquid jets. *Chem. Eng. Sci.* **36,** 1161–1172.

Ozawa, Y. and Mori, K. (1982) Observation of gas jets into a thin sheet of liquid metal. *Tetsu-to-Hagane* **68**, 90–97 (in Japanese) .

Sahai, Y. and Pierre, G. R. St (1992) *Advances in Transport Processes in Metallurgical Systems*. Amsterdam, Elsevier.

Shakouchi, T., Uejima, T., Ota, H. and Sato, S. (1995) Behavior of round plunging water jet. *14th Multiphase Flow Symposium '95*, Ehime, 39–42 (in Japanese) .

Shakouchi, T., Akita, T., Uejima, T., Ota, H. and Sato, S. (1996) The flow characteristics of round plunging water jet. *15th Multiphase Flow Symposium '96*, Fukui, 101–104 (in Japanese).

Tadaki, T. and Maeda, S. (1963) The size of bubbles from single orifices. *Kagaku Kogaku*, **27**, 147–155 (in Japanese) .

Wygnanski, I. and Fiedler, H. (1969) Some measurements in the self-reserving jet. *J. Fluid Mech.* **38,** 577–612.